Electron-impact study of NeF using the *R*-matrix method

Savinder Kaur* and K. L. Baluja†
Department of Physics and Astrophysics, University of Delhi, Delhi 110007, India

Jonathan Tennyson‡
Department of Physics and Astronomy, University College London, London WC1E6BT, United Kingdom

(Received 8 October 2007; published 20 March 2008)

Noble gas-halogen complexes form the basis of possible excimer lasers. Electron collisions are investigated with the prototypical neon fluoride molecule as a function of internuclear separation. The study concentrates on the four states making up the excimer system: The low-lying $X\ ^2\Sigma^+$ and $A\ ^2\Pi$ repulsive states and the high-lying $1\ ^2\Sigma^+$ and $2\ ^2\Pi$ charge-transfer states which can support bound states. These states are represented using a configuration-interaction expansion which is shown to yield accurate potential energy curves and target properties. Elastic and inelastic collision cross sections for the four states are calculated *ab initio* using the *R*-matrix method. Special care is needed to treat the large dipole moments found for the charge-transfer states which are predicted to have electron collision cross sections almost two orders of magnitude bigger than the lower states. Differential and momentum transfer cross sections are also considered for the electron impact on the repulsive ground state. Rate constants for electron deexcitation of the excimer states of NeF have been calculated for electron temperature corresponding up to 10 eV. The superelastic processes are dominated by the $1\ ^2\Sigma^+ \rightarrow X\ ^2\Sigma^+$ transition with thermal rate constant of $(2-5)\times 10^{-9}$ cm^3 s^{-1} in the entire range of electron temperature considered.

DOI: 10.1103/PhysRevA.77.032718 PACS number(s): 34.80.Bm, 34.80.Gs, 34.80.Ht

I. INTRODUCTION

Noble gas monohalides offer interesting possibilities for production of new ultraviolet lasers [1]. These excimer systems work on the principle that one or more of the electronically excited states can support bound rotation-vibration states while the ground state is weakly bound. This means that preparing any significant population in the upper state leads directly to population inversion.

Like many laser systems, one means of preparing the excimer system is by using an electric discharge to produce the necessary halogen atoms. This means that one can expect these excimer systems to exist with a background of free electrons. To our knowledge however the electron collision properties of these systems has never been studied. This is despite the fact that the very large dipole moments found in the (charge-transfer) excited states should lead to large electron collision cross sections. The population of charge-transfer excimers will probably be very low compared to the population of other strong scatterers, especially positive ions, so it seems unlikely they will much affect electron transport; however, their electron-impact deexcitation cross sections may be intrinsically interesting. In this paper we address the issue of low energy collisions with a potential excimer system.

The noble gas halogen excimer laser complexes have been well studied due to their potential as uv lasers [2–7]. This near to vacuum ultraviolet emission is of importance for many photochemical applications including laser isotope separation [8]. It could also be important for studying the dynamics of photodissociation in clusters and solid matrices, the transport properties of open-shell atoms in nonreactive baths and the role of long-range forces in chemical reactivity [9].

For this study we focus on neon fluoride, NeF, as this is electronically the simplest of the possible noble gas halide excimer lasing systems. The ground electronic state of NeF is very weakly bound; conversely several of the excited electronic states are very strongly bound as the excitation involves the transfer of an electron from the noble gas atom to the halogen atom. The emission features are characterized as due to charge-transfer transitions from a strongly ionic bonding upper state to a repulsive or weakly bound covalent lower state [10]. This large change in dipole moment leads to a correspondingly large transition moment between the ground and the two low-lying excited charge-transfer states. This suggests that NeF should provide a good laser medium [11].

Theoretical spectroscopic studies of the NeF molecule have been performed at several levels of approximation [11–15]. Burcl *et al.* [9] investigated the lowest states of Σ^+ and Π symmetry of $Rg\cdots Cl$ (Rg=He, Ne, Ar) complexes while Hoffman and Colleto [11] performed calculations on some noble gas monohalides, using the coupled cluster approach with single, double and noniterative triple excitations in an extended basis set including bond functions. Hartree-Fock self-consistent-field (HF-SCF) calculations for the $X\ ^2\Sigma^+$ and the $A\ ^2\Pi$ of NeF were performed by Gardner *et al.* [12]. They reported HF energies and dipole moments for the lowest $X\ ^2\Sigma^+$ and the $A\ ^2\Pi$ curves of NeF. Krauss [13] analyzed the rare gas halide excimer states in terms of an electrostatic model that includes mixing between the ionic excimer and neutral ground configurations. Winter *et al.* [14]

*Also at SGTB Khalsa College, Physics and Electronics Department, University of Delhi; sk_savinder2005@yahoo.co.in
†kl_baluja@yahoo.com
‡j.tennyson@ucl.ac.uk

characterized the emission spectra of NeF theoretically using accurate configuration-interaction potential energy curves. An early noteworthy study of NeF are the *ab initio* configuration-interaction calculations on the electronic states of *Rg*F (Rg=Ne, Ar, Kr, and Xe) arising from the covalent and ionic separated atom limits by Dunning and Hay [15].

The neon monohalides are less well studied experimentally due to very short wavelength for their fluorescence. An efficient laser in the 107 nm wavelength region would be useful as a photolytic source for the production of $O(^1S)$ from CO_2 [16]. However Rice *et al.* [17] predicted spontaneous emission of NeF^* at 108 nm providing motivation for experimental investigation.

Various lasing transitions have been observed using electron-beam excitation of mixtures of noble gases with compounds containing halogens and halogen molecules [17]. Becker *et al.* [18] performed studies on the interaction potentials for $F(^2P)$+Ne, Ar, $Kr(^1S)$ using crossed molecular beam.

The goal of this study is to calculate the *ab initio* potential energy curves for the four lowest states of NeF with Σ^+ and Π symmetry, i.e., the $X\ ^2\Sigma^+$ and $A\ ^2\Pi$ states, which correlate asymptotically with Ne and F in their ground states, and the $1\ ^2\Sigma^+$ and $2\ ^2\Pi$ states, which correlate with the lowest $Ne^+ + F^-$ asymptote; and to report differential and momentum cross sections for electron impact on NeF molecule in its ground state and excitation to the excited states. We also calculate superelastic cross sections from which we have the desired deexcitation rates. The calculations use the U.K. molecular *R*-matrix code [19,20]. The *R*-matrix method has the ability to provide a good representation of electron correlation in several excited states of the molecule [21]. There are a number of previous *R*-matrix calculations of cross sections for electron impact on various free radicals including Cl_xO_y species [22–24], CH and SH radicals [25,26], CF_x radicals [27,28], and the SF_2 radical [29].

II. METHOD

A. Theory

Since the *R*-matrix theory has been described in detail elsewhere [30,31], we only give an outline here. In an *R*-matrix approach, there are two distinct physically separated spatial regions, an inner region and an outer region, that are defined with respect to electron-molecule distances. These are treated differently in accordance with the different forces operating in each region. The center of the sphere coincides with the center of mass of the molecule. When the scattering electron leaves the inner region, the other target electrons are confined to the inner region.

Here the *R*-matrix boundary radius was chosen to be $10a_0$ centered at the NeF center of mass; the resulting sphere encloses the entire charge density of the molecule so that the amplitudes of the various occupied and virtual target orbitals are negligible at the boundary. However, the continuum orbitals have finite amplitudes. In the present case, the target boundary amplitudes at $10a_0$ are less than $10^{-9}a_0^{-3/2}$ for the occupied and virtual orbitals. Inside the *R*-matrix sphere, the electron-electron correlation and exchange interactions are strong. Short-range correlation effects are important for accurate prediction of large angle elastic scattering and exchange effects are important for spin-forbidden excitation cross sections.

A multicentered configuration-interaction (CI) wavefunction expansion is used in the inner region. The calculation in the inner region is similar to a bound-state calculation, which involves the solution of an eigenvalue problem for $(N+1)$ electrons in the truncated space, where there are N target electrons and a single scattering electron. Outside the sphere, only long-range multipolar interactions between the scattering electron and the various target states are included. Since only direct potentials are involved in the outer region, a single center approach is used to describe the scattering electron via a set of coupled differential equations. The *R* matrix is essentially a bridge between the two regions. It describes how the scattering electron enters the inner region and how it leaves it. In the outer region, the *R* matrix on the boundary is propagated outwards [32,33] until the inner region solutions can be matched with asymptotic solutions thus yielding the physical observables, such as cross sections.

In the polyatomic implementation of the U.K. molecular *R*-matrix code [19,20], the continuum molecular orbitals are constructed from atomic Gaussian-type orbitals (GTOs) using basis functions centered on the center of gravity of the molecule. The main advantage of GTOs is that integrals involving them over all space can be evaluated analytically in closed form. However, a tail contribution is subtracted to yield the required integrals in the truncated space defined by the inner region [19].

The target molecular orbital space is divided into core (inactive), valence (active) and virtual orbitals. The target molecular orbitals are supplemented with a set of continuum orbitals, centered on the center of gravity of the molecule. The continuum basis functions used in polyatomic *R*-matrix calculations are Gaussian functions and do not require fixed boundary conditions. First, target and continuum molecular orbitals are orthogonalized using Schmidt orthogonalization. Then symmetric or Löwdin orthogonalization is used to orthogonalize the continuum molecular orbitals among themselves and remove linearly dependent functions [19,34]. In general and in this work, all calculations are performed within the fixed-nuclei approximation.

In the inner region, the wave function of the scattering system consisting of target plus scattering electron is written using the configuration-interaction expression

$$\Psi_k^{N+1} = A\sum_i \phi_i^N(x_1, \ldots, x_N)\sum_j \xi_j(x_{N+1})a_{ijk} + \sum_m \chi_m(x_1, \ldots, x_N, x_{N+1})b_{mk}, \quad (1)$$

where A is an antisymmetrization operator, x_N is the spatial and spin coordinate of the Nth electron, ϕ_i^N represents the ith state of the N-electron target, ξ_j is a continuum orbital spin coupled with the scattering electron, k refers to a particular *R*-matrix basis function. Coefficients a_{ijk} and b_{mk} are variational parameters determined as a result of the matrix diagonalization.

TABLE I. Dominant configuration, dipole moment in a.u., transition moment of each transition from the ground state in a.u., the number of CI configurations, N, and the vertical excitation energies in eV for the target states of NeF at bond length $R=3.8a_0$.

State $C_{2v}/C_{\infty v}$	Dominant configuration	Dipole moment	Transition moment	N	Vertical excitation energy This work	Vertical excitation energy CI[a]
$X\ ^2A_1/X\ ^2\Sigma^+$	$1\sigma^2 2\sigma^2 3\sigma^2 4\sigma^2(5\sigma^2 6\sigma)1\pi^4 2\pi^4$	0.06355		495	0.000	0.000
$A\ ^2B_2/A\ ^2\Pi$	$1\sigma^2 2\sigma^2 3\sigma^2 4\sigma^2 5\sigma^2 6\sigma^2(1\pi^4 2\pi^3)$	0.03409	0.00627	366	0.466	0.569
$1\ ^2A_1/1\ ^2\Sigma^+$	$1\sigma^2 2\sigma^2 3\sigma^2 4\sigma^2(5\sigma 6\sigma^2)1\pi^4 2\pi^4$	3.63869	0.18730	495	11.228	10.967
$2\ ^2B_2/2\ ^2\Pi$	$1\sigma^2 2\sigma^2 3\sigma^2 4\sigma^2 5\sigma^2 6\sigma^2(1\pi^3 2\pi^4)$	3.70892	0.01706	366	11.483	11.297

[a]Winter *et al.* [14].

The first sum runs over the four target states included in the present calculation which are represented by a CI expansion. It accounts for one electron in a continuum state with the remaining electrons in a target state. To obtain reliable results, it is important to maintain a balance between the N-electron target representation, ϕ_i^N, and the $(N+1)$-electron scattering wave function. The summation in the second term of Eq. (1) runs over configurations χ_m, where all electrons are placed in target occupied and virtual molecular orbitals. The choice of appropriate χ_m is crucial [35]. These are known as L^2 configurations and are needed, since molecular orbitals are orthogonal, to account for orthogonality relaxation and for correlation effects arising from virtual excitation to higher electronic states that are excluded in the first expansion. The basis for the continuum electron is parametrically dependent on the R-matrix radius and provides a good approximation to an equivalent basis of orthonormal spherical Bessel functions [36].

B. NeF target model

NeF is a linear open-shell molecule whose ground state is $X\ ^2\Sigma^+$ in the $C_{\infty v}$ point group. However, we treat this molecule in a lower symmetry C_{2v} which is a subgroup of the highest group D_{2h} that is available in the polyatomic version of the code. However, all results are reported in the natural symmetry point group. We used a double zeta plus polarization (DZP) Gaussian basis set [37] contracted as (10,5,1)/(4,2,1) for Ne and (9,5,1)/(4,2,1) for F. We cannot use a basis set with very diffuse functions as this would extend outside the R-matrix box. We first performed a SCF calculation for the ground state of the NeF molecule with the chosen DZP basis set and obtained a set of occupied and virtual set of orbitals. The energies of the occupied molecular orbitals $1a_1$, $2a_1$, $3a_1$, $4a_1$, $5a_1$, $1b_1$, $1b_2$, $2b_1$, $2b_2$, and $6a_1$ are −892.11, −717.69, −52.69, −42.56, −23.46, −23.33, −23.33, −18.92, −18.92, and −11.12 eV, respectively, at bond length of $R=3.8a_0$.

We investigated spectroscopy of the NeF molecule with different bond lengths lying in the range $1.2-10a_0$. The Hartree-Fock electronic configuration for the ground state is $1\sigma^2 2\sigma^2 3\sigma^2 4\sigma^2(5\sigma^2 6\sigma)1\pi^4 2\pi^4$. Since the SCF procedure is inadequate to provide a good representation of the target states, we improve the energy of the ground as well as the excited states using CI. This lowers the energies and the correlation introduced provides a better description of the target wave function and excitation energies. In our limited CI model, we keep two core electrons frozen in the 1σ molecular orbitals. The remaining 17 electrons are free to move in 2σ, 3σ, 4σ, 5σ, 6σ, 1π, and 2π orbitals. This limited complete active space (CAS) CI model includes the dominant configurations for the excited states, see Table I. It was augmented by including additional configuration state functions arising from the promotion of one electron from the CAS to the external $7\sigma,\ldots,16\sigma$, $3\pi,\ldots,6\pi$ orbitals. The CI ground-state energy for NeF molecule is $-227.916\ 209\ 9E_h$, $-227.929\ 457\ 2E_h$, and $-227.934\ 248E_h$ at bond lengths $R=3.4a_0$, $3.8a_0$, and $4.2a_0$, respectively. A graphical representation of the potential energies with the bond length is exhibited in Fig. 1.

The lasing transition occurs between an ionic upper state and a covalent lower state. The lower two states arise from the $Ne(^1S)+F(^2P)$ separated atom limit and are essentially unbound. The upper two states correlate with $Ne^+(^2P)+F^-(^1S)$ ionic limit and are bound due to long-range Coulomb attraction of the ion pair. There is a large transition moment between the ground state and the two charge-transfer states. The bonding properties of the upper and

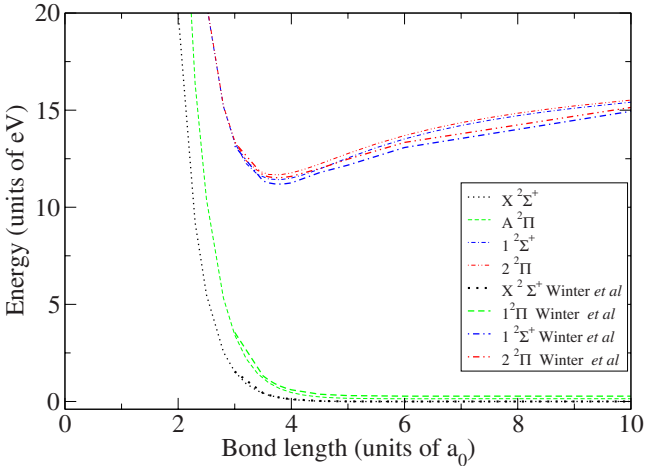

FIG. 1. (Color online) Potential energy curve for NeF: Dotted curve, $X\ ^2\Sigma^+$; dashed curve, $A\ ^2\Pi$; dashed-dotted curve, $1\ ^2\Sigma^+$; and dashed-double-dotted curve, $2\ ^2\Pi$

lower states guarantee a population inversion. It is a bound-free ionic-covalent transition.

To provide additional information on the charge distribution in the NeF molecule, we have also calculated the dipole and quadrupole moments at several geometries. We find for the CI model and $R=3.4a_0$, $3.8a_0$, and $4.2a_0$, respectively, the dipole moments are $0.326\,58D$, $0.161\,41D$, and $0.083\,75D$, and the absolute values of quadrupole component Q_{20} for the ground state are $-0.531\,26$ a.u., $-0.608\,868$ a.u., and $-0.650\,48$ a.u.

In Table I, we list the dominant configuration, the number of configuration state functions (CSFs), the dipole moments, the transition moments, and the vertical excitation energies for the target states. Our vertical transition energies are in good accord with the CI values of Winter *et al.* [14].

C. Scattering model

Our calculations included the four target states $X\,^2\Sigma^+$, $A\,^2\Pi$, $1\,^2\Sigma^+$, and $2\,^2\Pi$ in the close-coupling expansion of the wave function of the scattering system. Calculations were performed for singlet and triplet states with A_1, A_2, B_1, and B_2 symmetries. Continuum orbitals up to $l=4$ (g-partial wave) were represented by Gaussians centered at the molecule center of gravity [36].

Due to the presence of the long-range dipole interaction, the elastic cross sections are formally divergent in the fixed-nuclei approximation as the differential cross section is singular in the forward direction. To obtain converged cross sections, the effect of rotation must be included along with a very large number of partial waves. The effects of partial waves with $l>4$ were included using a Born correction via a closure approach. There are two approaches to make Born correction. In the first approach, a closure formula is used at the partial cross-section level, and in the second approach, the correction is applied at the T-matrix level. Both of these methods have been used in the present work. The correction at the cross-section level requires expressions for the partial as well as full Born cross sections. The closure approximation requires the evaluation of partial cross section σ_l^R and σ_l^B in the R matrix and Born approximation, respectively, for all the partial values up to g wave and then the integrated Born cross section, σ^B, is added as follows to obtain the Born corrected cross section σ:

$$\sigma = \sum_{l=0}^{4} (\sigma_l^R - \sigma_l^B) + \sigma^B. \tag{2}$$

In order to circumvent the problem of singularity in the Born cross section, we evaluate the rotational cross section ($j \rightarrow j'$) for initial rotor state $j=0$ to final rotor state $j'=1$. The expression for σ^B for this transition is simply given by

$$\sigma^B = \frac{8\pi}{3}\frac{D^2}{k_i^2}\ln\frac{k_i+k_f}{k_i-k_f}. \tag{3}$$

The partial cross section for dipole allowed σ_l^B in the Born approximation for $j=0$ to $j'=1$ transition is given by Eq. (17) of Chu and Dalgarno [38]. This involves the evaluation of a $3j$ coefficient and the radial matrix element $I_{ll'}$ given by

$$I_{ll'} = \int_0^\infty j_l(k_i r) j_{l'}(k_f r) dr \tag{4}$$

which involves the evaluation of hypergeometric function.

Finally, the expression for σ_l^B is simplified as

$$\sigma_l^B = \frac{16\pi}{3} D^2 \frac{k_f}{k_i}(2l+1)\sum_{l'}(2l'+1)(C(ll'1;000))^2(I_{ll'})^2 \tag{5}$$

where, D is the relevant dipole (transition) moment in a.u. for the ground (excited) state and k_i (k_f) are initial and final momentum of the impinging electron. The rotational energy is $2B$ for $0 \rightarrow 1$ transition, where B is the rotational constant of NeF at a particular geometry. The expression (5) is taken from Chu and Dalgarno [38]. The Born contribution for partial waves higher than $l>4$ to the ground-state elastic cross section at energies below 5 eV is quite small owing to small dipole moments but is larger for the charge-transfer states. In the second approach, the T matrices are initially subjected to a frame transformation to laboratory frame and the Born correction is applied to the resulting rotationally resolved T matrices. The program POLYDCS of Sanna and Gianturco [39] was used for this purpose as well as for calculating rotationally elastic and inelastic differential cross sections from our four-state K matrices. Both the approaches yielded similar results. In the energy range 2–10 eV, the elastic cross section for the ground state differ by less than one-half percent. In fact, we also performed the entire R-matrix calculation using partial waves up to $l=3$. From this, and our g-wave results, we calculated the contribution of only the g wave in the R-matrix approach. This result was compared with the corresponding Born result. Both the results are close to each other. At 0.1 eV, there is a difference of only 0.025%. As the energy increases, the contribution of g wave also decreases but there is good agreement between the g-wave partial cross section of R-matrix and Born results. This establishes the correctness of our procedure to use Born correction beyond g-partial wave. Due to the multicenter nature of the inner region the results are found to be insensitive if we change the cutoff from g-partial wave to f-partial wave. For elastic scattering from excited states, that have sizable dipole moments, we estimate that our cross sections may be higher by about 5% for all the excited states studied here. Born corrections were also included in the inelastic cross sections since all transitions considered are dipole allowed; however the corrections are generally small for these due to higher thresholds.

The maximum number of coupled channels in our scattering calculation is 30. A channel is described by coupling the symmetry of a particular target state with a particular symmetry component describing the scattered electron. The number of CSFs for a typical singlet (triplet) scattering symmetry is around 1800. Due to the large dipole moments of the excited state we have propagated the R matrix to a radius of $70a_0$.

III. RESULTS

Figure 1 shows the variation of potential energy for the ground $X\ ^2\Sigma^+$ and the three excited states: $A\ ^2\Pi$, $1\ ^2\Sigma^+$, and $2\ ^2\Pi$ with the internuclear separation of NeF. The potential curves of the $X\ ^2\Sigma^+$ and $A\ ^2\Pi$ states are repulsive with only a slight van der Waals minimum, while the $1\ ^2\Sigma^+$ and $2\ ^2\Pi$ curves are attractive because of the Coulombic attraction between the Ne^+ and F^- ions. This binding is independent of the symmetry of the state and hence we expect both ionic states to be strongly bound and at larger internuclear distances they are nearly degenerate. The potential curve of the $X\ ^2\Sigma^+$ state is substantially less repulsive than the $A\ ^2\Pi$ state. This was also observed by Dunning and Hay [15]. The $X\ ^2\Sigma^+$ and $A\ ^2\Pi$ states separate rapidly at small R, whereas the $1\ ^2\Sigma^+$ and $2\ ^2\Pi$ states remain nearly degenerate. The contribution of ionic configuration in the wave function of the $X\ ^2\Sigma^+$ is approximately given by μ/R_e which at $R_e(2\ ^2\Sigma^+)$ is only about 1.7%.

The potential energies for the NeF electronic states at different bond lengths are in good agreement with HF calculations of Gardner *et al.* [12] and CI calculations of Winter *et al.* [14]. A comparison of the potential well with the CI calculation of Winter *et al.* [14] is also exhibited in Fig. 1.

The separation of ionic and covalent asymptotic limits is simply the difference between the ionization potential of Ne (21.565 eV) and the electron affinity of F (3.401 eV), which is 18.164 eV [40,41]. Our value of 18.13 eV is in close agreement with this. Our calculation predicts a transition at 110.5 nm at a bond length of $3.8a_0$ compared to the 107 nm value of Ewing and Brau [2]. An emission feature at 108 nm observed in electron beam excited Ne-F_2 mixtures has been attributed to NeF by Rice *et al.* [17]

Figure 2 shows the variation of dipole moment and the quadrupole moments of the ground and excited states as a function of bond length. The dipole moment is compared with the result of Winter *et al.* [14] and shows good agreement. The curve of the ground state has the correct behavior, showing that the dipole moment approaches zero at the united- and separated-atom limits. The large amount of charge transfer in the upper states is evident in the large values of the dipole moment for these states whose dipole moment is nearly equal to R in atomic units.

In Figs. 3 and 4 we present the elastic cross sections at $3.4a_0$, $3.8a_0$, and $4.2a_0$ for the ground state and at $3.8a_0$ for the excited state, respectively, for the NeF molecule at low energy. In all cases, for energies below 2 eV the cross sections rise rapidly due to the dipolar interactions; these are particularly marked for the charge-transfer states. For the ground state between 2 eV and 12 eV, the cross sections are nearly constant around $45a_0^2$, which reflects the dominance of quadrupole interactions. The cross sections are higher for higher bond length due to larger Q values. While the elastic cross section for the covalent $A\ ^2\Pi$ state is similar to that of the ground state, those for the ionic states are almost two orders of magnitude larger. For these states the large dipole moment is the dominant interaction and use of the Born correction leads to a significant increase in the cross section.

Figure 5 presents electron-impact excitation cross sections from the ground state $X\ ^2\Sigma^+$ to the $A\ ^2\Pi$, $1\ ^2\Sigma^+$, and $2\ ^2\Pi$ excited states, respectively, for $R=3.4a_0$, $3.8a_0$, and $4.2a_0$. The cross sections for the $^2\Pi$ target states show rapid increase at thresholds. For the $A\ ^2\Pi$ state, the cross section increases as bond length increase in contrast to the behavior for excitation to the $1\ ^2\Sigma^+$ and $2\ ^2\Pi$ target state. The cross section for the excited state $1\ ^2\Sigma^+$ rise linearly with increasing energy for all the bond lengths as shown in Fig. 5. We included the Born correction for the excitation cross sections for the excited states but the only noticeable change was for excitation to $1\ ^2\Sigma^+$ state, and even this was not too significant.

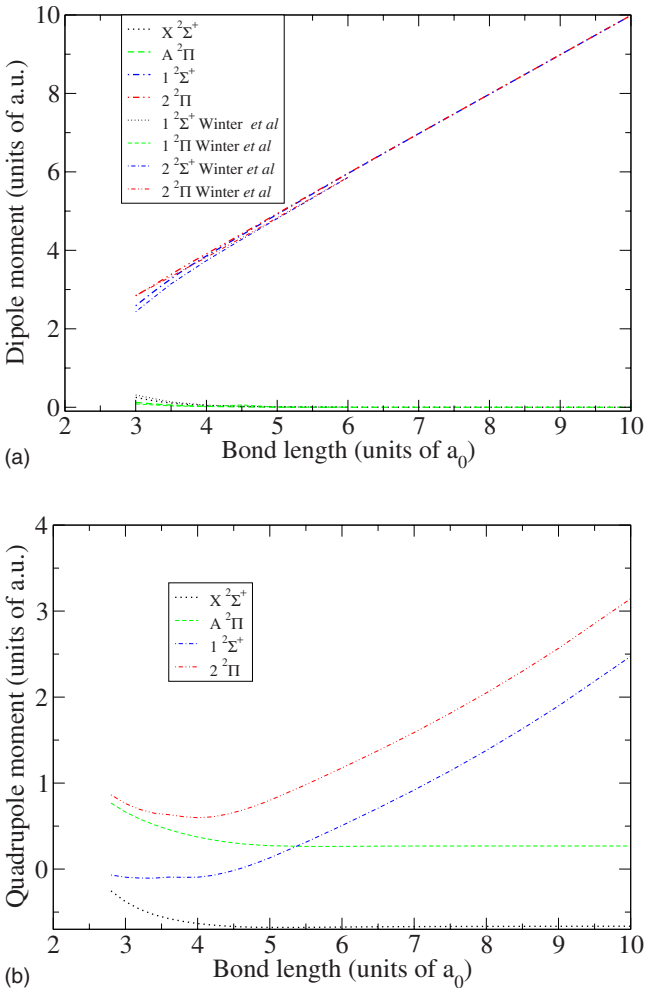

FIG. 2. (Color online) Dipole moment (upper) and quadrupole moment (lower) as a function of bond length of the ground and excited states. Dotted curve, $X\ ^2\Sigma^+$; dashed curve, $A\ ^2\Pi$, dashed-dotted curve, $1\ ^2\Sigma^+$, and dashed-double-dotted curve, $2\ ^2\Pi$.

One can infer the superelastic, i.e., downward, cross sections, σ_{ji}, from the electron impact electronic excitation cross sections, σ_{ij}, given above using the principle of detailed balance. At an incident electron energy E they are related by the formula

$$\sigma_{ji}(E-\Delta) = \frac{g_i}{g_j}\sigma_{ij}(E)[1-(\Delta/E)]^{-1}, \tag{6}$$

where Δ is the excitation energy of the transition $i \rightarrow j$. Hazi *et al.* [42] theoretically studied the deexcitation of KrF and

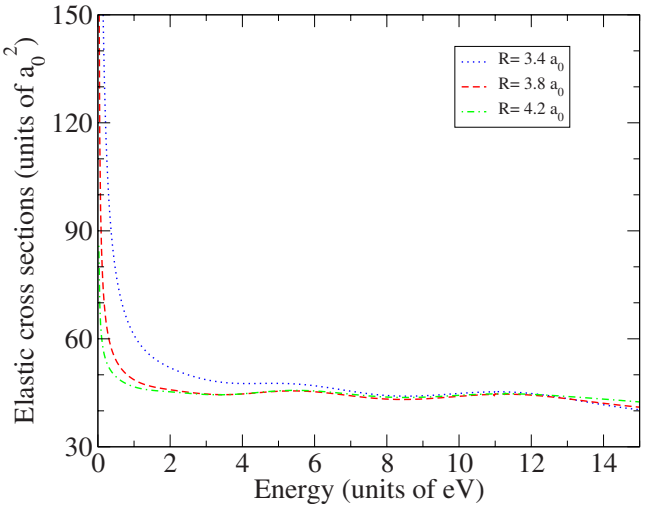

FIG. 3. (Color online) Ground-state elastic cross sections of the NeF molecule at different bond lengths: Dotted curve, $R=3.4a_0$; dashed curve, $R=3.8a_0$; dotted-dashed curve, $R=4.2a_0$.

XeF excimers using a modified impact parameter method.

We also calculated the rate coefficients for the deexcitation of the NeF excimer at bond length of $3.8a_0$ assuming Maxwell-Boltzmann distribution to obtain the temperature-dependent rate coefficients for the $A\ ^2\Pi \rightarrow X\ ^2\Sigma^+$, $1\ ^2\Sigma^+ \rightarrow X\ ^2\Sigma^+$, $2\ ^2\Pi \rightarrow X\ ^2\Sigma^+$, $1\ ^2\Sigma^+ \rightarrow A\ ^2\Pi$, $2\ ^2\Pi \rightarrow A\ ^2\Pi$, $2\ ^2\Pi \rightarrow 1\ ^2\Sigma^+$ transitions. In Fig. 6, these have been plotted as a function of electron temperature. These have been evaluated by using the principle of detailed balancing and are given by

$$C_{ji} = \frac{g_i}{g_j} C_{ij} \exp^{E_{ij}/kT} \ (\mathrm{cm}^3\ \mathrm{s}^{-1}), \tag{7}$$

where, C_{ji} and C_{ij} are the deexcitation rate coefficients and the excitation coefficient rates, respectively. E_{ij} is the excess energy, g_i and g_j are the degeneracy's of the initial and final state, respectively. It is evident that the electron deactivation of the excimer states is dominated by the $1\ ^2\Sigma^+ \rightarrow X\ ^2\Sigma^+$ transition with rate coefficient lying in the range of $(2-5) \times 10^{-9}\ \mathrm{cm}^3\ \mathrm{s}^{-1}$. The deexcitation rates for $A\ ^2\Pi \rightarrow X\ ^2\Sigma^+$ is lower by a factor of 3 than the above transition. This is in conformity with the work of Hazi *et al.* [42] for KrF and XeF excimers. The other deexcitation rates are smaller.

Figure 7 displays our calculated differential cross section (DCS) for electron scattering by ground-state NeF at incident energies of 2, 5, 7, and 10 eV. We present results for $R=3.8a_0$ which is the bond length where the excited states $1\ ^2\Sigma^+$ and $2\ ^2\Pi$ show a minimum in the potential energy curve. Due to lack of other data on DCS at low energies, we are limited in our discussion on the quality of our DCS. The sharp enhancement in the forward direction is a well-known result of the long-range dipole component of the interaction potential. The combined effects of correlation in the target states and the effect of close-channel effects may be responsible for the differences in the angular region of 10°–50° at various energies. We did not detect any resonances, either shape or Feshbach, in our scattering calculations. This is probably due to the fact that the ground state of NeF^- is an

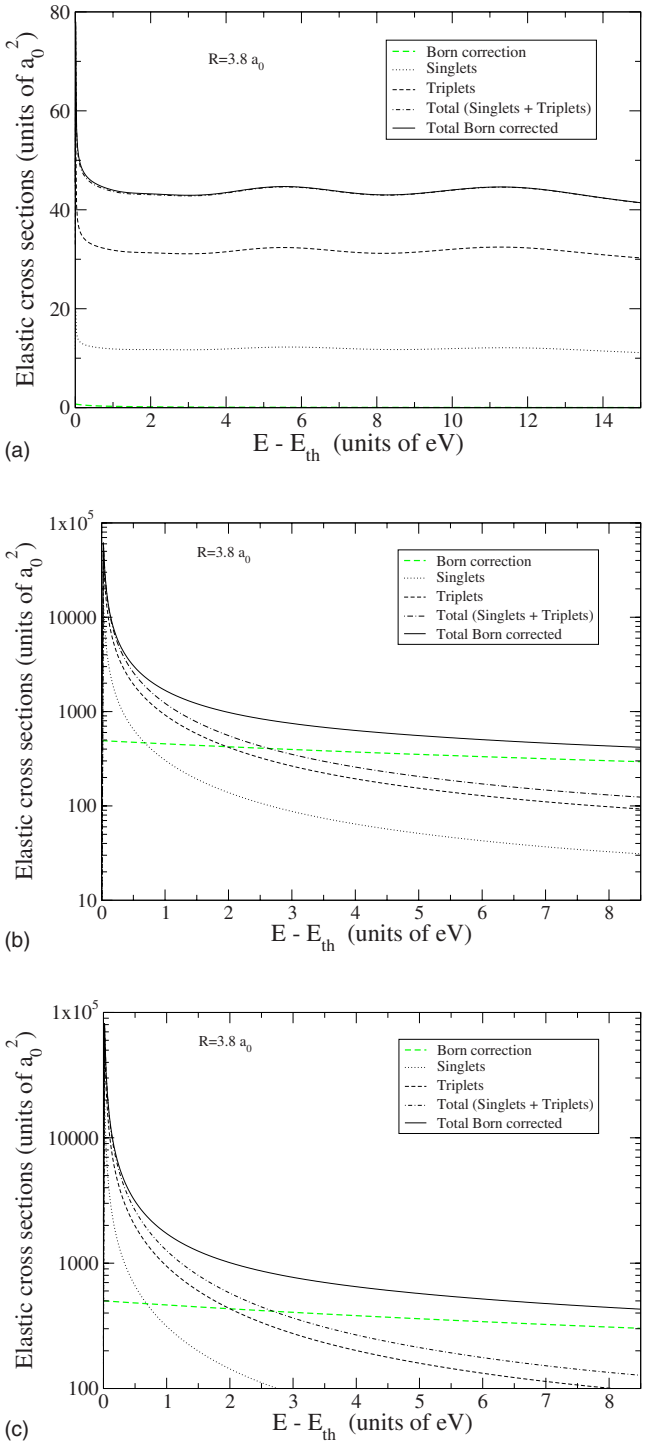

FIG. 4. (Color online) Elastic cross sections for $A\ ^2\Pi$ (upper), $1\ ^2\Sigma^+$ (middle), and $2\ ^2\Pi$ (lower) states of the NeF molecule at fixed bond length $R=3.8a_0$.

electronically bound closed-shell system whose excited states lie at high energy and may, indeed, not even be temporarily stable. Indeed our calculations found that the $X\ ^1\Sigma^+$ ground state of NeF^- is bound by 1.61 eV at $R=3.8a_0$.

In Fig. 8, the results for the momentum transfer cross sections (MTCS) for ground-state NeF are presented in the range 1 eV to 10 eV at the bond length of $3.8a_0$. The MTCS

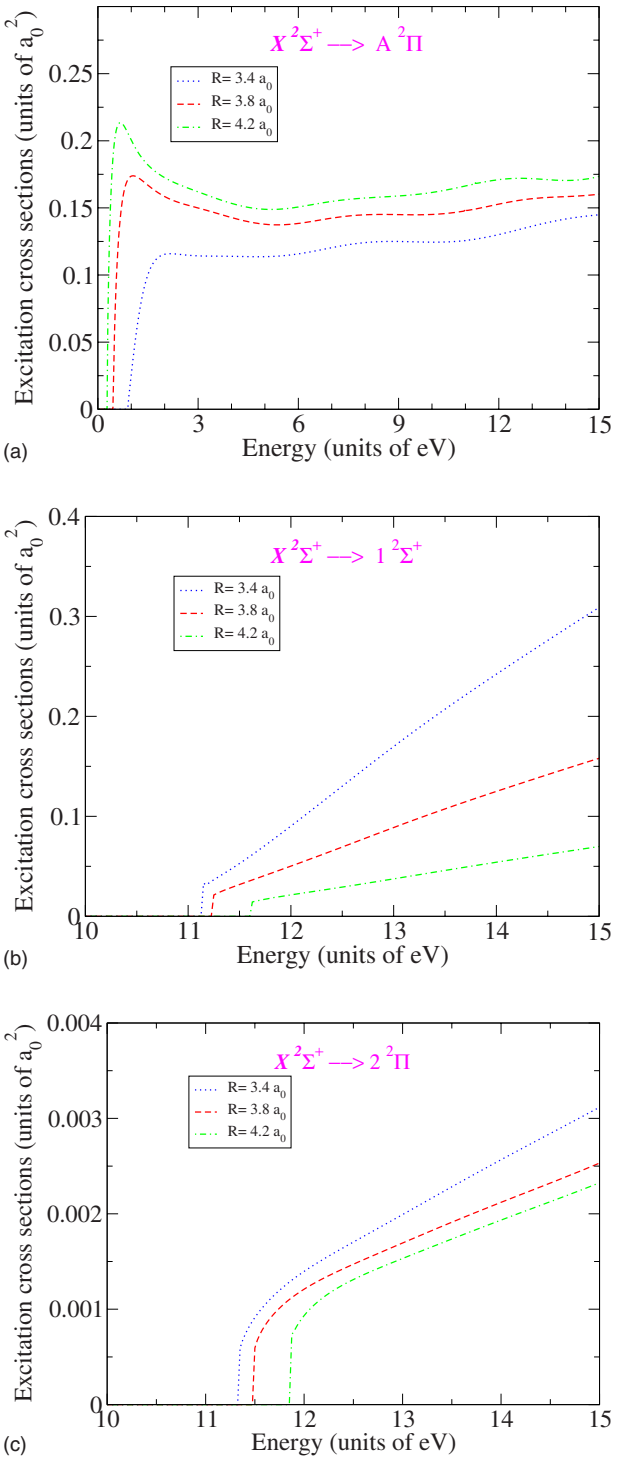

FIG. 5. (Color online) Electron impact excitation cross sections from the ground $X\ ^2\Sigma^+$ state of the NeF molecule to the $A\ ^2\Pi$ state (top), the $1\ ^2\Sigma^+$ state (middle), and the $2\ ^2\Pi$ state (bottom) at different internuclear separation, R.

is an indication of the amount of backward scattering. The MTCS is a useful observable for swarm study of electrons through gases and it determines the electron distribution function through the solution of Boltzmann equation and their drift velocity in the molecular gas. This may be important for modeling electron transport properties in the NeF

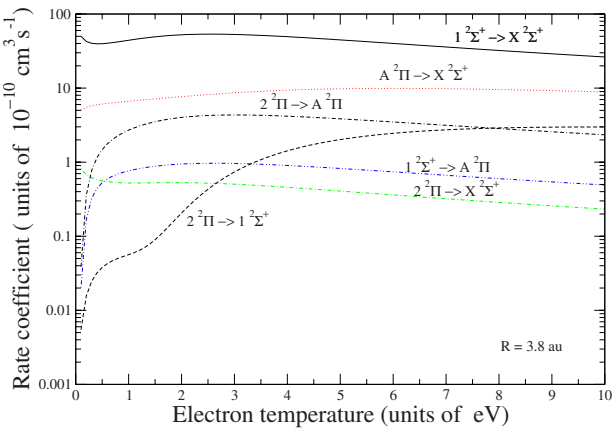

FIG. 6. (Color online) Calculated rate coefficients for the electron deexcitation of NeF excimer. A Maxwell-Boltzmann distribution of electrons is assumed. Dotted curve, $A\ ^2\Pi \rightarrow X\ ^2\Sigma^+$; solid curve, $1\ ^2\Sigma^+ \rightarrow X\ ^2\Sigma^+$; dashed-dotted curve, $2\ ^2\Pi \rightarrow X\ ^2\Sigma^+$; dashed-double-dotted curve, $1\ ^2\Sigma^+ \rightarrow A\ ^2\Pi$; double-dashed-dotted curve, $2\ ^2\Pi \rightarrow A\ ^2\Pi$; and dashed curve, $2\ ^2\Pi \rightarrow 1\ ^2\Sigma^+$.

excimer laser. We observe that MTCS decrease with increasing incident energies. In contrast to the divergent nature of the DCS at lower angles the MTCS do not diverge due to the weighting factor of $(1-\cos\theta)$.

IV. CONCLUSIONS

This paper is a study on electron scattering by the NeF molecule and is based on the *ab initio R*-matrix method. Our target calculations give reasonable agreement with the calculated vertical excitation spectrum of Winter *et al.* [14]. We also obtain good agreement with the value of the ground-state dipole moment with other works [12,14]. The good target representation are crucial for obtaining reliable results [35]. Previous benchmark studies on dipolar systems (e.g., [43,44]) suggest that the ground-state elastic, integral, differ-

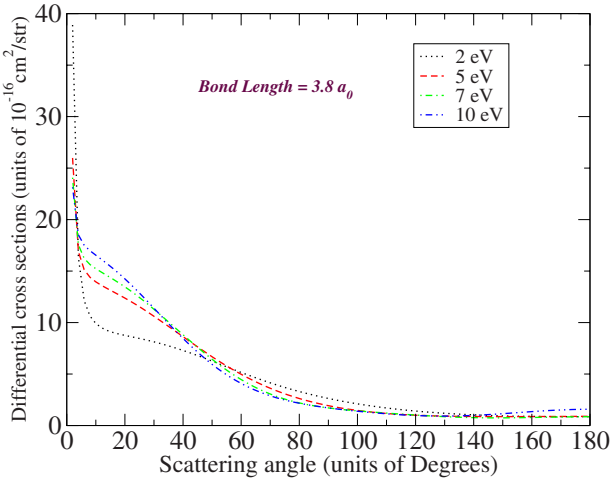

FIG. 7. (Color online) Differential cross sections at 2, 5, 7, and 10 eV at bond length of $3.8a_0$ of the NeF molecule ground state.

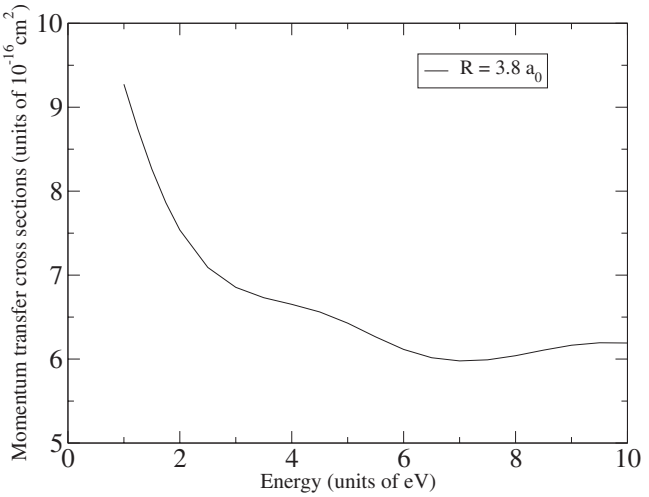

FIG. 8. Momentum transfer cross sections at different energies for $R=3.8a_0$ of NeF molecule ground state.

ential, and momentum transfer cross sections presented here should be of high quality.

Given the unusual nature of the NeF excimer system we have also considered elastic cross sections for the excited states. For these there are no benchmark studies to provide comparisons. However collisions with the bound charge-transfer states are dominated by the large permanent dipoles possessed by these states; a situation which should yield reliable *ab initio* results.

We have chosen to present electron impact excitation cross sections from the ground electronic state since these are usual cross sections considered. However, we note that as the ground state is unstable, the more likely inelastic process is superelastic: Electron impact deexcitation of the excited states. The cross sections for this reverse process are obtained using the principle of detailed balance. The dominant deexcitation rate coefficient is for the transition $1\ ^2\Sigma^+ \rightarrow X\ ^2\Sigma^+$ and is in the range of $(2-5)\times 10^{-9}$ cm^3 s^{-1}. At normal electron densities, this may be comparable to other quenching processes.

We hope that the results presented here will not only be useful for comparison with future experimental studies but will also provide data useful in models of the NeF excimer laser.

ACKNOWLEDGMENT

We thank the Royal Society for supporting this work via a Joint Project grant.

[1] A. M. Boichenko, V. F. Tarasenko, and S. I. Yakovlenko, Laser Phys. **10**, 1159 (2000).
[2] J. J. Ewing and C. A. Brau, Appl. Phys. Lett. **27**, 350 (1975).
[3] J. M. Hoffman, A. K. Hays, and G. C. Tisone, Appl. Phys. Lett. **28**, 538 (1976).
[4] C. A. Brau and J. J. Ewing, Appl. Phys. Lett. **27**, 435 (1975).
[5] P. C. Tellinghuisen, J. Tellinghuisen, J. A. Coxon, J. E. Velazo, and D. W. Setser, J. Chem. Phys. **68**, 5187 (1978).
[6] G. Inoue, J. K. Ku, and D. W. Setser, J. Chem. Phys. **80**, 6006 (1984).
[7] M. Boivineau, J. Le Calv, M. C. Castex, and C. Jouvet, Chem. Phys. Lett. **128**, 528 (1986).
[8] V. S. Letokhov, Annu. Rev. Phys. Chem. **28**, 133 (1977).
[9] R. Burcl, R. V. Krems, A. A. Buchachenko, M. M. Szczesniak, G. Chalasinski, and S. M. Cybulski, J. Chem. Phys. **109**, 2144 (1998).
[10] T. H. Dunning and P. J. Hay, Appl. Phys. Lett. **28**, 649 (1976).
[11] G. J. Hoffman and M. Colleto, J. Chem. Phys. **114**, 2219 (2001).
[12] M. A. Gardner, A. M. Karo, and A. C. Wah, J. Chem. Phys. **65**, 1222 (1976).
[13] M. Krauss, J. Chem. Phys. **67**, 1712 (1977).
[14] N. W. Winter, C. F. Bender, and T. N. Rescigno, J. Chem. Phys. **67**, 3122 (1977).
[15] T. H. Dunning, Jr. and P. J. Hay, J. Chem. Phys. **69**, 134 (1978).
[16] J. J. Ewing and C. A. Brau, Phys. Rev. A **12**, 129 (1975).
[17] J. K. Rice, A. K. Hays, and J. R. Woodworth, Appl. Phys. Lett. **31**, 31 (1977).
[18] C. H. Becker, P. Casavecchia, and Y. T. Lee, J. Chem. Phys. **70**, 2986 (1979).
[19] L. A. Morgan, C. J. Gillan, J. Tennyson, and X. Chen, J. Phys. B **30**, 4087 (1997).
[20] L. A. Morgan, J. Tennyson, and C. J. Gillan, Comput. Phys. Commun. **114**, 120 (1998).
[21] J. Tennyson, J. Phys. B **29**, 1817 (1996).
[22] K. L. Baluja, N. J. Mason, L. A. Morgan, and J. Tennyson, J. Phys. B **33**, L677 (2000).
[23] K. L. Baluja, N. J. Mason, L. A. Morgan, and J. Tennyson, J. Phys. B **34**, 2807 (2001).
[24] K. L. Baluja, N. J. Mason, L. A. Morgan, and J. Tennyson, J. Phys. B **34**, 4041 (2001).
[25] K. L. Baluja and A. Z. Msezane, J. Phys. B **34**, 3157 (2001).
[26] K. L. Baluja and A. Z. Msezane, J. Phys. B **35**, 437 (2002).
[27] I. Rozum, N. J. Mason, and J. Tennyson, J. Phys. B **35**, 1583 (2002).
[28] I. Rozum, N. J. Mason, and J. Tennyson, New J. Phys. **5**, 155 (2003).
[29] K. L. Baluja and J. A. Tossell, J. Phys. B **37**, 609 (2004).
[30] P. G. Burke and K. A. Berrington, *Atomic and Molecular Processes: An R-Matrix Approach* (Institute of Physics, Bristol, 1993).
[31] C. J. Gillan, J. Tennyson, and P. G. Burke, in *Computational Methods for Electron-Molecule Collisions*, edited by W. M. Huo and F. A. Gianturco (Plenum, New York, 1995).
[32] K. L. Baluja, P. G. Burke, and L. A. Morgan, Comput. Phys. Commun. **27**, 299 (1982).
[33] L. A. Morgan, Comput. Phys. Commun. **31**, 419 (1984).
[34] B. M. Nestmann, K. Pfingst, and S. D. Peyerimhoff, J. Phys. B **27**, 2297 (1994).

[35] J. Tennyson, J. Phys. B **29**, 6185 (1996).
[36] A. Faure, J. D. Gorfinkiel, L. A. Morgan, and J. Tennyson, Comput. Phys. Commun. **144**, 224 (2002).
[37] T. H. Dunning and P. J. Hay, in *Methods of Electronic Structure Theory*, edited by H. F. Schaefer (Plenum, New York, 1977), Vol. 2.
[38] S. I. Chu and A. Dalgarno, Phys. Rev. A **10**, 788 (1974).
[39] N. Sanna and F. A. Gianturco, Comput. Phys. Commun. **114**, 142 (1998).
[40] C. E. Moore, *Atomic Energy Levels*, Natl. Bur. Stand. (U.S.) Circ. 467, Vol. 1 (U.S. GPO, Washington, DC, 1949)
[41] R. S. Berry and C. W. Riemann, J. Chem. Phys. **38**, 1540 (1963).
[42] A. U. Hazi, T. N. Rescigno, and A. E. Orel, Appl. Phys. Lett. **35**, 477 (1979).
[43] M. Gupta and K. L. Baluja, J. Phys. B **38**, 4057 (2005).
[44] M. Gupta and K. L. Baluja, Phys. Rev. A **73**, 042702 (2006).